Isotropic and anisotropic regimes of the field-dependent spin dynamics in Sr_{2}IrO_{4}: Raman scattering studies

Y. Gim, A. Sethi, Q. Zhao, J. F. Mitchell, G. Cao, and S. L. Cooper

Phys. Rev. B **93**, 024405 — Published 11 January 2016

DOI: 10.1103/PhysRevB.93.024405

Isotropic and Anisotropic Regimes of the Field-Dependent Spin Dynamics in Sr_2IrO_4: Raman Scattering Studies

Y. Gim,[1] A. Sethi,[1] Q. Zhao,[2] J. F. Mitchell,[2] G. Cao,[3,4] and S. L. Cooper[1]

[1] *Department of Physics and Frederick Seitz Materials Research Laboratory, University of Illinois, Urbana, Illinois 61801, USA*

[2] *Material Science Division, Argonne National Laboratory, Argonne, Illinois 60439, USA*

[3] *Center for Advanced Materials, University of Kentucky, Lexington, Kentucky 40506, USA*

[4] *Department of Physics and Astronomy, University of Kentucky, Lexington, Kentucky, 40506, USA*

A major focus of experimental interest in Sr_2IrO_4 has been to clarify how the magnetic excitations of this strongly spin-orbit coupled system differ from the predictions of an isotropic 2D spin-1/2 Heisenberg model and to explore the extent to which strong spin-orbit coupling affects the magnetic properties of iridates. Here, we present a high-resolution inelastic light (Raman) scattering study of the low energy magnetic excitation spectrum of Sr_2IrO_4 and doped Eu-doped Sr_2IrO_4 as functions of both temperature and applied magnetic field. We show that the high-field (H>1.5 T) in-plane spin dynamics of Sr_2IrO_4 are isotropic and governed by the interplay between the applied field and the small in-plane ferromagnetic spin components induced by the Dzyaloshinskii-Moriya interaction. However, the spin dynamics of Sr_2IrO_4 at lower fields (H<1.5 T) exhibit important effects associated with interlayer coupling and in-plane anisotropy, including a spin-flop transition at H_c in Sr_2IrO_4 that occurs either discontinuously or via a continuous rotation of the spins, depending upon the in-plane orientation of the applied field. These results show that in-plane anisotropy and interlayer coupling effects play important roles in the low-field magnetic and dynamical properties of Sr_2IrO_4.

PACS numbers: 75.30.Ds,75.30.Kz,75.50.Ee,78.30.-j

I. INTRODUCTION

The 5d iridates have attracted much recent attention, because the comparable spin-orbit coupling and electronic correlation energy scales in these materials are expected to be conducive to exotic phases and phenomena, such as superconductivity,[1,2] spin-liquid states,[3] a J_{eff}=1/2 Mott state,[4,5] topological phases,[6–8] and magneto-electric behavior.[9] The antiferromagnetic insulator, Sr_2IrO_4 (T_N∼240 K),[10–12] is of particular interest, because the strong spin-orbit coupling in this iridate contributes significantly to its insulating behavior:[4,5] The Ir^{4+} ($5d^5$) ions in Sr_2IrO_4 provide 5 d-electrons that occupy the t_{2g} states, which are well separated from higher-energy e_g bands by crystal-field effects. The spin-orbit interaction λ ∼0.4 eV further splits the t_{2g} levels into half-filled J_{eff}=1/2 and filled J_{eff}=3/2 bands. Insulating behavior is thought to arise because of on-site Coulomb interactions, which split the J_{eff}=1/2 level into upper and lower Hubbard bands. This general picture is supported by angle-resolved photoemission, optical conductivity, and x-ray absorption measurements.[4,13]

An important unresolved issue concerns the extent to which the strongly entangled spin-orbit states comprising the J_{eff}=1/2 Ir 5d moments influence both the magnetic properties and the magnetic excitation spectrum of Sr_2IrO_4.[4,5,14] Neutron scattering studies[12,15] have shown that Sr_2IrO_4 has an antiferromagnetic configuration with a ∼11° canting of the AF spins in the ab-plane, associated with the antisymmetric Dzyaloshinskii-Moriya (DM) spin exchange anisotropy in Sr_2IrO_4. This in-plane canting leads to net ferromagnetic in-plane moments (see Fig. 1(c)), m_{FM} ≈$0.06\mu_B$,[16,17] that are antiferromagnetically coupled along the c-axis in a (↑↓↓↑) pattern.[5]

However, while the static magnetic configuration of Sr_2IrO_4 has been well established, the magnetic excitation spectrum of this strongly spin-orbit-coupled system has not been so well characterized. In particular, it is not clear whether the magnetic excitations associated with the spin-orbit entangled J_{eff}=1/2 moments in Sr_2IrO_4 can be described by the predictions of an isotropic S=1/2 Heisenberg model.[16,18,19] Unfortunately, inelastic neutron scattering studies of the magnetic excitations in Sr_2IrO_4 are hampered by the strong absorption of neutrons by Ir.[19] Resonant inelastic x-ray scattering (RIXS) studies of Sr_2IrO_4 have probed both low-energy charge[20] and magnetic[14,21] excitations, but the relatively low resolution associated with RIXS measurements have not allowed a detailed study of the low energy magnetic excitations that would reveal deviations from Heisenberg model predictions. Interestingly, recent resonant magnetic diffuse x-ray[16] and field-dependent electron spin resonance[17] studies of Sr_2IrO_4 have offered evidence that the magnetic correlations and excitations are well-described by the two-dimensional S=1/2 Heisenberg model, in spite of the strong spin-orbital coupling associated with the Ir 5d moments.

In this paper, we present an inelastic light (Raman) scattering study of the low energy magnetic excitation spectrum of Sr_2IrO_4 and doped Eu-doped Sr_2IrO_4 as functions of temperature, applied magnetic field, and magnetic field orientation. Inelastic light scattering is a valuable probe for studying the spin-dynamics of Sr_2IrO_4: This technique is a very high resolution probe of the $\mathbf{q}$=0 magnetic excitation energies, which are influenced by small anisotropy and inter-

layer coupling interactions that can uncover physics beyond the isotropic, two-dimensional S=1/2 Heisenberg model description.[22–25] Additionally, Raman scattering can probe the spin dynamics both with and without an applied field. Consequently, this technique is useful for studies of spin dynamics in the interesting low-field region of Sr_2IrO_4, particularly through the field-induced antiferromagnetic (AF) to weakly ferromagnetic (WFM) spin-flop transition at $H_c \approx 0.15$ T.[5,10]

In the results reported here, we show that the in-plane spin dynamics of Sr_2IrO_4 at high fields (H>1.5 T) are well-described by isotropic, two-dimensional S=1/2 Heisenberg model predictions. By contrast, the low-field (H<1.5 T) spin dynamics of Sr_2IrO_4 exhibit important effects associated with interlayer coupling and in-plane anisotropy that are not accounted for in standard descriptions of the spin-dynamics of Sr_2IrO_4. These effects include an anisotropic field-dependence of the spin-dynamics for H<1.5 T, and an AF-to-WFM transition that occurs via either discontinuous spin-flop or continuous spin-reorientation transitions for different in-plane field orientations.

II. EXPERIMENTAL SET UP

A. Sample Preparation

The single crystals of Sr_2IrO_4 ($T_N \sim 240$K) studied were grown from off-stoichiometric quantities of $SrCl_2$, $SrCO_3$ and IrO_2 using self-flux techniques. Technical details are described elsewhere.[10] The structures of Sr_2IrO_4 samples were determined using a Nonius Kappa CCD X-ray diffractometer. The data were collected between 90 K and 300 K, and the structures were refined using the SHELX-97 program.[26] Chemical compositions of the single crystals were determined using energy dispersive X-ray analysis (EDX) (Hitachi/Oxford 3000).

The Eu-doped Sr_2IrO_4 sample ($T_N \sim 200$K) was synthesized at Argonne National Laboratory using a Eu-enriched $SrCl_2$ flux method. Samples were characterized by DC magnetization using a Quantum Design SQUID magnetometer.[27]

The samples were cleaved to create c-axis normal surfaces, as verified using room temperature x-ray diffraction measurements.

B. Raman Measurements

Raman scattering measurements were performed using the 647.1 nm excitation line from a Kr^+ laser. The incident laser power was limited to 5 mW and was focused to a ~ 50 μm-diameter spot to minimize laser heating of the samples. The scattered light from the samples was collected in a backscattering geometry, dispersed through a triple stage spectrometer, and then detected with a liquid-nitrogen-cooled CCD detector. The incident light polarization was selected with a combination of a polarization rotator and a 1/4-waveplate and the scattered light polarization was analyzed with a linear polarizer. The scattering geometry used for all measurements had both the incident and scattered polarizations oriented in the ab-planes of the crystals. The incident and scattered light polarizations, $\mathbf{e}_i$ and $\mathbf{e}_s$, were kept in a $(\mathbf{e}_i,\mathbf{e}_s)$=(R,x) configuration for all measurements, where R represents right circular polarized light and x represents linear polarized light oriented in the ab-planes of the crystals.

The samples were inserted into a continuous He-flow cryostat, which was horizontally mounted in the open bore of a superconducting magnet. This experimental arrangement allowed Raman scattering measurements under the simultaneous conditions of low temperature (3-290 K) and high magnetic field (0-8 Tesla). Field-dependent Raman measurements were performed after zero-field cooling the samples to T$\sim$3 K in order to avoid inducing the antiferromagnetic (AF) to weakly ferromagnetic (WFM) alignment of the ferromagnetic spin components in adjacent layers, which occurs for very low critical fields ($H_c \sim 0.15$ T) in Sr_2IrO_4.[5,10]

Temperature- and field-dependent Raman scattering measurements were performed on two different Sr_2IrO_4 samples and one Eu-doped Sr_2IrO_4 sample. The two Sr_2IrO_4 samples studied−one of which was used to obtain the temperature-dependent data of Fig. 1(a) and the second of which was used to obtain the field-dependent data shown in Fig. 2-4−exhibited slightly different spin-wave energies (on the order of 1 cm^{-1} or 0.13 meV energy difference). However, the qualitative temperature- and field-dependences of the spin-wave excitation energies were nearly identical in both Sr_2IrO_4 samples. In addition to the spin-wave excitations, a temperature- and field-independent peak was observed in many of the spectra near 29 cm^{-1} (peaks denoted with asterisks (*) in the H=0 T spectra of Fig. 2(a) and 3(a)). This 29 cm^{-1} peak is associated with unfiltered light from the laser and was fit and subtracted from the spectra at other fields so the field-dependences of the spin-wave excitations could be more clearly observed. Because of the very narrow linewidth of the 29 cm^{-1} peak, its subtraction from the spectra did not affect our determination of the spin-wave energies at different magnetic fields. Note that the higher frequency phonon spectra of the samples studied were also measured and the phonon results obtained were similar in most respects to results reported earlier.[28] However, the focus of this paper will be on the spin-wave excitation spectra of Sr_2IrO_4 and the phonon spectra will not be shown or discussed further here.

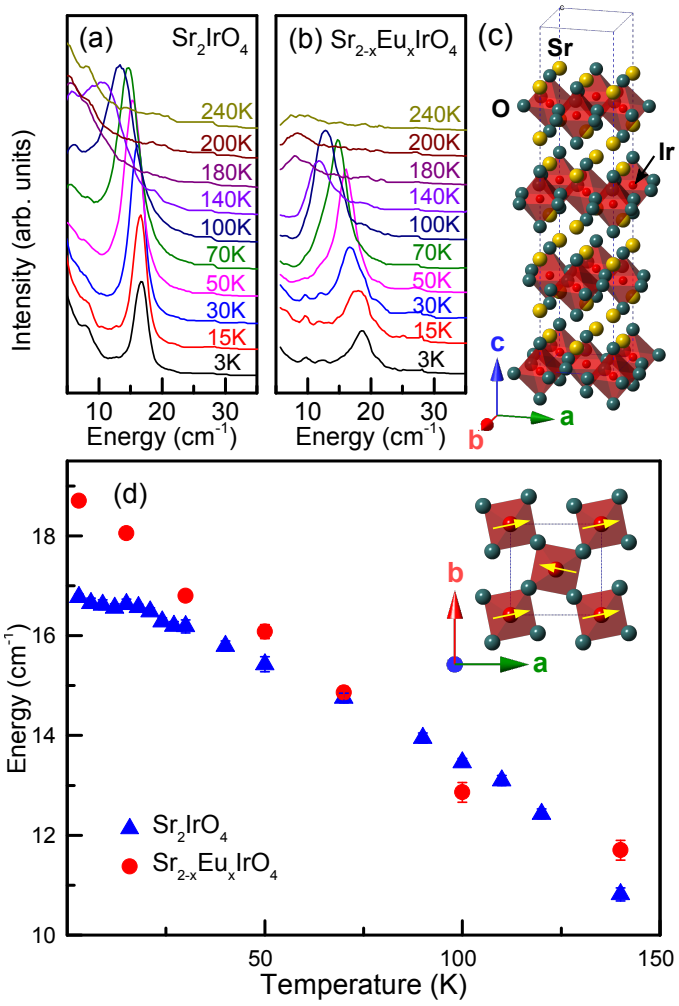

FIG. 1. Temperature dependence of the spin-wave spectra of (a) Sr_2IrO_4 and (b) Eu-doped Sr_2IrO_4. (c) Summary of the temperature dependence of spin-wave energies for Sr_2IrO_4 and Eu-doped Sr_2IrO_4. The left inset shows the crystal structure of Sr_2IrO_4. Because of octahedral rotations, the unit cell of Sr_2IrO_4 contains 4 layers of IrO_2. The right inset shows the in-plane orientations of the J_{eff}=1/2 moments.

III. RESULTS

A. Temperature- and Doping-dependent Results

Figure 1(a) shows the low frequency (5−35 cm^{-1}) excitation spectrum of Sr_2IrO_4 as a function of temperature for H=0 T. At temperatures near T_N ∼240 K, the low energy spectrum exhibits a diffusive background, most likely associated with incoherent spin scattering. Below T_N, this diffusive background develops into a sharp mode that increases in energy with decreasing temperature to a slightly sample-dependent value near ω_2∼17-18 cm^{-1} (2.1-2.3 meV) at T=3 K. Additionally, a weak second peak near ω_1=9-10 cm^{-1} is observed in the 3 K spectrum; this lower-energy mode is more clearly observed in the second Sr_2IrO_4 sample used for the field dependent measurements (see Fig. 2) and will be discussed in more detail in the field-dependent results section below.

The effects of doping on the low energy magnetic excitation spectrum of Sr_2IrO_4 are also shown in Fig. 1(b), which displays the temperature dependence of the ∼18 cm^{-1} spin wave excitation near in Eu-doped Sr_2IrO_4. The temperature dependences of the spin-wave energies in Eu-doped Sr_2IrO_4 (filled circles) and Sr_2IrO_4 (filled triangles) are summarized in Fig. 1(c). Several slight differences between the spin wave modes in the doped and undoped Sr_2IrO_4 samples are observed: the linewidths of the ∼18 cm^{-1} spin wave mode are slightly broader in the doped sample compared to the undoped sample ($\Gamma_{doped}/\Gamma_{undoped}$ ≈1.25), which is likely associated with greater spin and potential disorder in the doped sample. The doped sample also exhibits a slightly higher value for the spin-wave mode energy at T=3 K, but this difference is consistent with the sample-to-sample variations we noted for the measured spin-wave energies in undoped Sr_2IrO_4; consequently, this energy difference is not believed to be significant. Thus, the most noteworthy feature of Fig. 1(b) is that there is not a substantial influence of slight doping on the **q**=0 spin-wave energies in Sr_2IrO_4. This conclusion is consistent with evidence that electron doping in Sr_2IrO_4 causes a subtle unbuckling of the IrO_6 octahedra and a crossover to metallic behavior, but does not significantly affect the magnetic properties of Sr_2IrO_4.[11]

B. Field-dependent Results

Figure 2(a) shows the magnetic-field dependence of the spin-wave spectrum of Sr_2IrO_4 for a field orientation parallel to the FM moment (i.e., H‖b-axis=[010]). The field-dependent results for Eu-doped Sr_2IrO_4 are similar and will not be shown. Two spin-wave modes, ω_1 and ω_2, are clearly evident in the H=0 T spectrum at ω_1=11 cm^{-1} (1.38 meV) and ω_2=18 cm^{-1} (2.25 meV). As a first step towards identifying these modes, note that in the simplest description of Sr_2IrO_4 as a two-dimensional canted antiferromagnet−which ignores, in particular, interlayer coupling between the antiferromagnetically coupled layers[29]−the two-fold degenerate **q**=0 spin-wave branch is expected to split into a low-frequency "ferromagnetic (FM) mode" and a higher frequency "antiferromagnetic (AF) mode", associated with precession of the spins about the FM and AF axes, respectively.[17,23,30,31] However, we can likely rule out assigning either ω_1 or ω_2 to the FM mode of Sr_2IrO_4, because previous ESR measurements have reported that the FM spin-wave mode in Sr_2IrO_4 has an H≈0 T value of ω_{FM}=0.32 cm^{-1},[17] which is well below the spectral range of our light scattering study. We can also rule out the possibility that the modes at ω_1 and ω_2 in Fig. 1(a) are the same spin-wave mode associated with different magnetic domains in Sr_2IrO_4. Magnetic domains have been reported in

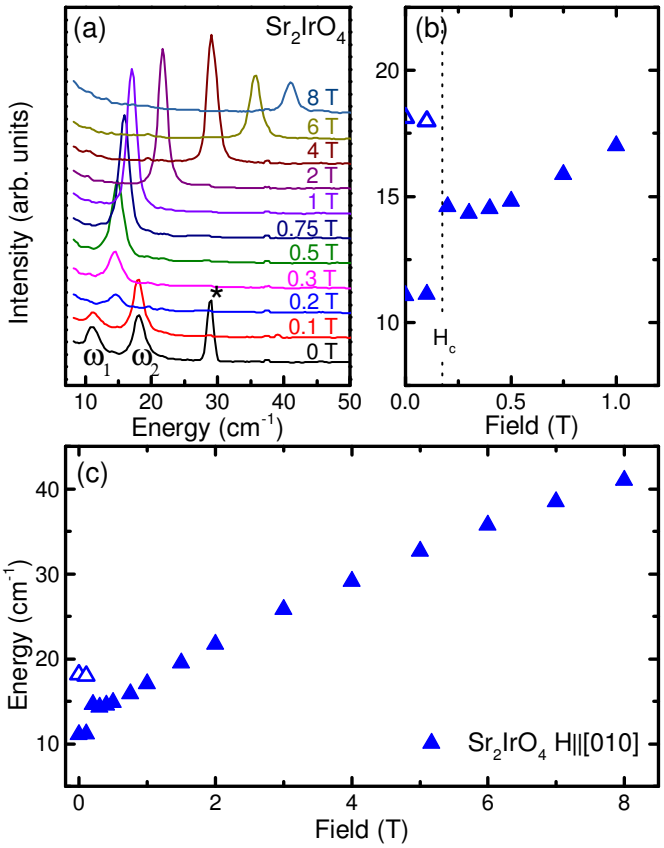

FIG. 2. Field dependence of spin-wave spectra of (a) Sr_2IrO_4 for H||b-axis (=[010]) at T=3 K. The peak marked with an asterisk (*) in the H=0 T spectra is an artifact from the laser and this peak has been removed from the spectra at other fields. The spectra have been offset for clarity. Summary of the field-dependence of the spin wave energies for ω_1 (filled triangles) and ω_2 (open triangles) in Sr_2IrO_4 with H||b-axis are shown in (b) (expanded view) and (c) (full range).

Sr_2IrO_4, but likely involve simple 90° rotations of the unit cell,[32] which cannot account for the significantly different energies (∼1 meV) of the ω_1 and ω_2 modes shown in Sr_2IrO_4 (see Fig. 2(a)). Magnetic domains with a different stacking sequence of the layers−such as domains already in the WFM phase at H=0 T−would cause the same spin-wave mode to have slightly different energies in the different domains. However, the energy difference in this case would probably not be large enough to account for the large (∼ 1 meV) observed energy difference between the ω_1 and ω_2 spin wave modes in Sr_2IrO_4. Further, to our knowledge there have been no reports that domains associated with the WFM phase are present at H=0 T in Sr_2IrO_4.

Therefore, the two spin-wave modes ω_1 and ω_2 in Fig. 2(a) are most likely associated with the effects of interlayer coupling between antiferromagnetically coupled IrO layers. As discussed by Thio et al. for La_2CuO_4,[33] interlayer coupling between the two inequivalent (antiferromagnetically coupled) layers in Sr_2IrO_4 results in a magnetic unit cell that contains four spins and two 2-fold FM and AF magnon branches whose degeneracies at H=0 T are split by interlayer coupling.[22] We associate the spin-wave modes ω_1 and ω_2 in Sr_2IrO_4 with the in-phase and out-of-phase combinations of the AF spin-waves on adjacent layers, respectively. This interpretation is supported by the observed reduction from two $\mathbf{q}$=0 AF spin-wave modes in the antiferromagnetic (AF) phase of Sr_2IrO_4−which has two magnetically inequivalent layers per unit cell in the simplest model description−to a single $\mathbf{q}$=0 AF spin-wave mode (see Figs. 2(a), 2(b), and 2(c)) in the weakly ferromagnetic (WFM) phase of Sr_2IrO_4, which has only a single layer per unit cell. In particular, in the WFM phase, the out-of-phase AF spin-wave mode ω_2 becomes a zone-boundary mode and only the in-phase AF mode ω_1 is expected to be present at $\mathbf{q}$=0.

The importance of interlayer coupling on the spin-wave excitation spectrum of Sr_2IrO_4 is also supported by the abrupt increase in the in-phase AF spin-wave energy (ω_1=3.4 cm^{-1} or 0.43 meV) (Figs. 2(b) and 2(c)) at H_c, which reflects an increase in the AF spin-wave stiffness through the AF-to-WFM transition. The energy shift of ω_1 at H_c allows an estimate of the interlayer coupling energy in Sr_2IrO_4: Using the measured change in the energy of ω_1 at H_c (see Fig. 2(b)) and the result that,[22,25]

$$4JJ_\perp = [\omega_1^2(H_c^+) - \omega_1^2(H_c^-)]/\sqrt{2} \qquad (1)$$

we find $4JJ_\perp$∼59 cm^{-2} in Sr_2IrO_4, giving an estimate for the value of the interlayer coupling energy $J_\perp$∼0.018 cm^{-1} (2.3 μeV) (using J∼800 cm^{-1}).[16] This estimate of $J_\perp$ is consistent with published reports for Sr_2IrO_4, including estimates based upon the measured critical field H_c in Sr_2IrO_4: $J_\perp = mH_c/S^2$,[22,29] which gives $J_\perp$∼3 μeV for Sr_2IrO_4, using m=0.07μ_B per Ir atom, H_c=0.15 T, and S=1/2.

The magnetic-field dependences of the AF spin-wave energies ω_1 and ω_2 of Sr_2IrO_4 are shown for different applied field orientations in Fig. 3. Figure 3(a) shows the magnetic field dependences of ω_1 and ω_2 with H roughly parallel to the spin direction, H||a-axis=[100], while Fig. 3(b) shows the magnetic field dependences of ω_1 and ω_2 with H oriented roughly 45° from the a-axis, i.e., H||[110]. Note that the H=0.4 T spectrum in Fig. 3 (a) and the summary plot in Fig. 4 (a) shows three peaks, consisting of a superposition between the two spin-wave modes of the AF phase and the single spin-wave mode in the WFM phase. This superposition is consistent with a coexistence of AF and WFM phases expected near the first-order transition at H_c.

Also shown in Fig. 3(c) is the magnetic field dependence of the $\mathbf{q}$=0 spin-wave spectrum in Sr_2IrO_4 for the out-of-plane magnetic field orientation, i.e., with H roughly parallel to the c-axis direction, H||[001]. The ω_1∼8 cm^{-1} (not shown) and ω_2∼18 cm^{-1} spin-wave mode energy exhibits a much weaker magnetic field de-

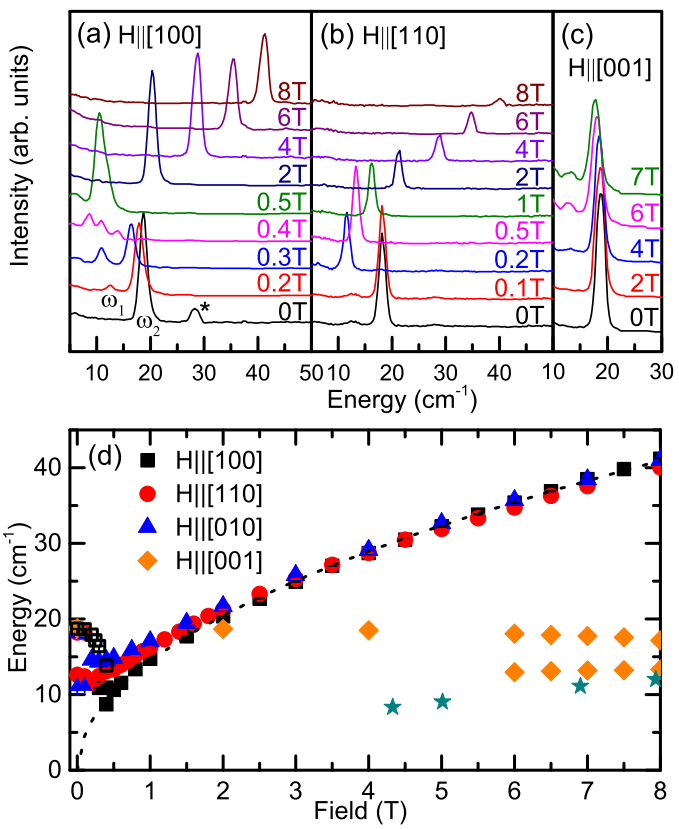

FIG. 3. Field dependences of the spin-wave spectra of Sr2IrO4 for (a) H||[100], (b) H||[110], and (c) H||[001] at T=3 K. The peak marked with an asterisk (*) in the H=0 T spectrum is an artifact from the laser and has been removed from the spectra at other fields. The spectra have been offset for clarity. (d) Summary of the field-dependences of the spin wave energies for different applied field orientations for both ω_1(filled symbols) and ω_2(open symbols). Also shown for comparison are results from ESR measurements[17] for H||[001] (filled stars). The dashed line is a fit to the data with the functional form $\omega=\sqrt{\gamma H}$ using γ=209.38 cm^{-2}T^{-1}.

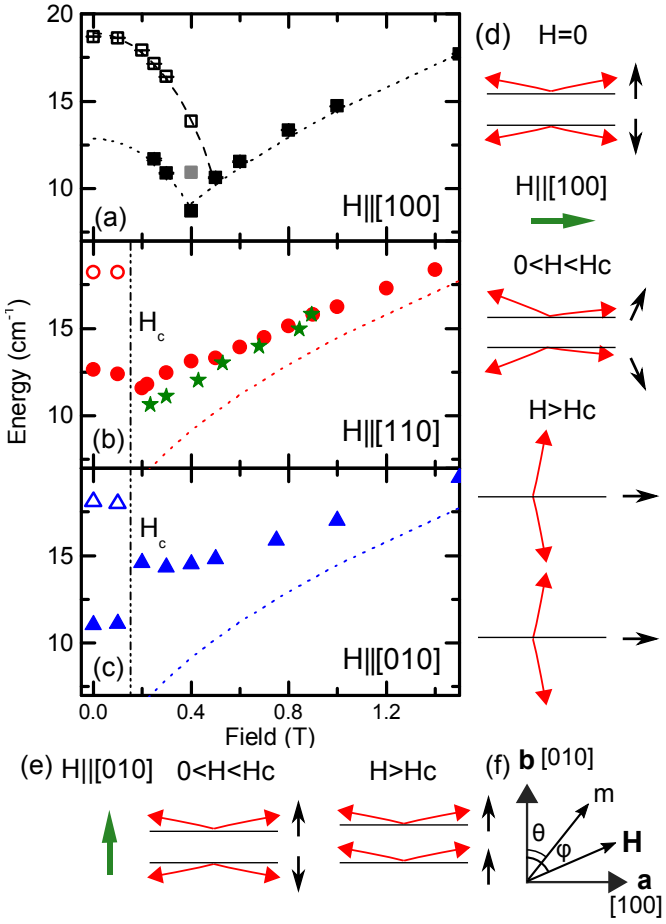

FIG. 4. Summaries of the field dependences of the spin-wave energies of Sr_2IrO_4 for different in-plane field orientations, including (a) H||a-axis=[100], (b) H||[110], and (c) H||b-axis=[010] at T=3 K. (Closed symbols= ω_1 mode, Open symbols= ω_2 mode) The dashed lines are plots of $\omega=\sqrt{\gamma H}$ with γ=209.38 cm^{-2}T^{-1} for comparison with the data. The long-dashed line is a fit to the data with the functional form of $\omega=\sqrt{\Delta^2-\alpha H^2}$ with Δ=18.9 cm^{-1} and α=1014 cm^{-2}T^{-2}. The dashed line below H<0.4T in (a) is also fitted with same functional form with Δ=12.8 cm^{-1} and α=542.9 cm^{-2}T^{-2}. Also shown for comparison are results from ESR measurements[17] for H||[110] (filled stars). The filled gray square at H=0.4 T in (a) represents the ω_1 mode in the WFM phase, which coexists at H=0.4 T with the ω_1 (filled black square) and ω_2 (open square) modes associated with the AFM phase. (d) Schematic illustration of the rotation of the staggered spin components (red arrows) and uniform spin component (black arrows) on adjacent layers for an applied field (green arrow) oriented transverse to easy axis direction of FM component of the spin, H||a-axis=[100], illustrating the continuous rotation of the spins on adjacent layers for this applied field orientation. (e) Schematic illustration of the rotation of the staggered spin components (red arrows) and uniform spin component (black arrows) on adjacent layers for an applied field (green arrow) oriented parallel to easy axis direction of FM component of the spin, H|| b-axis=[010], illustrating the abrupt flipping of the spins in one layer for this field orientation. (f) Diagram showing the angle θ of the FM component of the spins (**m**) and the angle ϕ of the applied field (H) relative to the easy axis in-plane orientation of **m** (i.e., [010]).

pendence for H||c-axis=[001], consistent with previous electron spin resonance (ESR) results (filled stars).[17] An additional weak mode develops near ∼13 cm $^{-1}$ for H>4 T with H||c-axis=[001]. This mode may be associated with the presence of a small in-plane field caused by a slight misalignment of the magnetic field in the H||c-axis configuration, which can induce an AF-to-WFM transition−and a lower value for the spin-wave energy (as discussed above)−in parts of the sample.

IV. DISCUSSION

The central result of this study concerns the magnetic-field-dependences (0≤H≤8 T) of the AF spin-wave mode energies summarized in Fig. 3(d) for different in-plane magnetic field orientations, H||a-axis=[100] (filled

squares), H‖b-axis=[010] (filled triangles), and H‖[110] (filled circles). Fig. 3(d) illustrates that there are 2 distinct field regimes for the in-plane spin dynamics in Sr_2IrO_4, (A) an isotropic regime for H$\gtrsim$1.5T and (B) an anisotropic regime for H$\lesssim$1.5T.

A. Isotropic regime H$\gtrsim$1.5T

For H>1.5 T, the in-plane spin dynamics are isotropic and the AF spin-wave mode ω_1 energy in the WFM phase region is well-described by a square-root field dependence, $\omega_1 = \sqrt{\gamma H}$, with γ=209.4 cm^{-2}T^{-1} (dashed line). The isotropic square-root field dependence for H>1.5 T indicates that the FM components of the spins simply follow the applied field direction in Sr_2IrO_4, due to the dominant interaction between the applied field and the weak FM moments induced by the DM interaction.[17,24,31]

The spin dynamics above H>1.5 T in Sr_2IrO_4 are consistent with an isotropic, two-dimensional effective S=1/2 Hamiltonian given by:[17,34]

$$H_{12} = J\vec{S_1}\cdot\vec{S_2} + \Gamma S_1^z S_2^z + D(S_1^x S_2^y - S_1^y S_2^x) \quad (2)$$

where the first term (J) is associated with isotropic antiferromagnetic exchange between the two inequivalent spins, 1 and 2, in the IrO plane, the second term (Γ) represents symmetric exchange anisotropy that favors collinear c-axis spin order, and the third term (D) represents antisymmetric exchange anisotropy that favors canted in-plane spin order. Bahr *et al.* predict that for Γ,D $\ll$ J, the AF spin-wave energy associated with the model Hamiltonian in Eq.(2) should have a field-dependence given by,[17]

$$\omega_1 \approx \sqrt{\Delta^2 + 8Jm_{FM}H} \quad (3)$$

where J$\sim$100 meV in Sr_2IrO_4, m_{FM} is the FM canting moment and Δ is the spin gap energy at H=0. This prediction is consistent with the square-root field dependence we observe for ω_1 in Fig. 3(d). Using our value of γ=209.4 cm^{-2}T^{-1} from the fit to the data in Fig. 3(d) (dashed line) with $\Delta\sim$ 0, we obtain an estimated FM canting moment of $m_{FM}\sim\gamma/8J \sim 0.07\mu_B$ in Sr_2IrO_4, which is consistent with other estimates (e.g., see ref. 16). Notably, the γ value determined from the field-dependence of the AF spin wave in La_2CuO_4 (γ_{LCO}= 22.6 cm$^{-2}T^{-1}$)[23] is much smaller than our value for Sr_2IrO_4, reflecting the much smaller FM moment associated with spin canting in La_2CuO_4 ($m_{FM}\sim0.002\mu_B$).[29]

B. Anisotropic regime H$\lesssim$1.5T

Figure 3(d) shows that the field-dependent spin-wave dynamics for H<1.5 T are highly anisotropic in the planes, revealing interaction effects in Sr_2IrO_4 that are not accounted for in Eq.(2). A more detailed view of the anisotropic magnetic field dependence of the AF spin wave energy in Sr_2IrO_4 is provided in Fig. 4, which shows the field-dependences of spin-wave energies ω_1 and ω_2 in the field range 0$\leq$H$\leq$1.5 T for several in-plane field orientations, including (a) H‖a-axis=[100], (b) H‖[110], and (c) H‖b-axis=[010]. As discussed above, Fig. 4(c) shows that the in-phase AF spin-wave energy ω_1 exhibits an abrupt increase in energy ($\Delta\omega_1$=3.4 cm^{-1} or 0.43 meV) through the AF-to-WFM spin-flop transition at $H_c\sim$0.15 T when the applied field is oriented in the direction of the FM (uniform) spin component of the spins, H‖b-axis=[010]. This behavior indicates that the AF-to-WFM transition in Sr_2IrO_4 occurs via a discontinuous spin-flop transition, and results in a discontinuous change in interlayer coupling, when the applied field is oriented along the weak FM component of the spins (see Fig. 4(e)).

On the other hand, when the applied field is oriented perpendicular to the FM spin component of the spins (i.e., parallel to the staggered spins), H‖a-axis=[100], Fig. 4(a) shows that when the applied field is oriented parallel to the staggered spins, H‖a-axis=[100], AF spin-wave modes ω_1 and ω_2 exhibit "soft mode" behavior: the field-dependence of ω_2 with H‖a-axis=[100] is well described by the functional form $\omega_2 = \sqrt{\Delta^2 - \alpha H^2}$ (long-dashed line) with Δ=18 cm^{-1} and α=1014 cm$^{-2}T^{-2}$. The soft spin-wave mode behavior shown in Fig. 4(a) indicates that the AF-to-WFM transition involves a continuous spin reorientation and a gradual crossover when H‖a-axis=[100] (Figure 4(d)). The field-dependence of the AF spin wave energy of Sr_2IrO_4 for H‖[110], shown in Fig. 4(b), exhibits behavior intermediate to that observed for the H‖[010] and H‖[100] orientations. Also shown for comparison in Fig. 4(b) is the field-dependence of the AF spin-wave mode ω_{AF} determined from electron-spin-resonance (ESR) measurements with H‖[110] (filled stars),[17] showing that there is a good agreement between the AF spin-wave energies measured with Raman scattering and ESR for this H‖[110] orientation.

The dramatic difference in the nature of the AF-to-WFM transition for different in-plane field orientations (Fig. 4) reflects the importance of in-plane anisotropy for H$\lesssim$1.5T in Sr_2IrO_4. Similar effects of in-plane anisotropy on the spin dynamics of ferrimagnets[35] and canted antiferromagnets[36–38] have been observed previously, particularly in iridates,[39] cuprates[33,38] and ferrites.[36,37,40–42] The AF spin-wave mode softening observed in Sr_2IrO_4 (Fig. 4(a)) reflects a continuous decrease in the interlayer exchange energy in Sr_2IrO_4 with applied field for H$\perp m_{FM}$, caused by the continuous field-induced rotation of the FM moments in opposite directions in the antiferromagnetically coupled layers (see Fig. 4(d)).

An estimate of the in-plane anisotropy field, H_A, can be obtained from our data by first developing a simple phenomenological description of the interlayer coupling energy between two adjacent layers, which can be written, $E_\perp\sim J_\perp\cos(2\theta)=J_\perp(1-2\sin^2(\theta))$, where θ is the angle between the FM spin components and their zero-field

(easy axis) directions in the each of two layers (see Fig. 4(f)). The interlayer coupling energy can be written in terms of the applied in-plane field H, using the result that the equilibrium in-plane orientation for the weak FM moment in each layer for a particular field H is given by:[38]

$$(H_{DM}/H_E)Hsin(\phi-\theta) = (H_A)sin(2\theta) \qquad (4)$$

where H_{DM} is the Dzyaloshinskii-Moriya field, H_E is the exchange field, H_A is the in-plane anisotropy field, H is the applied field, θ is the angle between the FM spin component, m_{FM}, and its zero-field (easy axis) orientation, ϕ is the angle between the applied field and the easy-axis, and assuming $H_E \gg H_{DM} \gg H_A \sim H$. Equation (4) shows that a field applied perpendicular to the easy-axis orientation of m_{FM} (i.e., $H \perp m_{FM}$ or $\phi=\pi/2$), which is the field orientation for which we observe soft magnon behavior (see Fig. 4(a)), induces an in-plane rotation of m_{FM} by an angle θ that increases continuously with the applied field according to $\sin(\theta)=(H_{DM}/2H_AH_E)H$, as schematically depicted in Fig. 4(d). In the AF phase, the ferromagnetic components in adjacent layers rotate in opposite directions in response to an applied transverse in-plane field. Consequently, the interplane exchange energy for a pair of coupled layers will continuously decrease with field H for $H<H_c$ according to $E_\perp \sim J_\perp(1-2\beta^2H^2)$, where $\beta=(H_{DM}/2H_EH_A)$. This functional form for $E_\perp$ is consistent with the observed field-dependences of the spin wave mode energies near H∼0.4 T for H‖a-axis=[100] (see Fig. 4(a)). Note that the interplane exchange energy goes to zero, $E_\perp \rightarrow 0$, at a critical field given by $H_c=\sqrt{2}(H_E/H_{DM})H_A$. Using our rough measurement of the field at which the AF spin-wave mode energy approaches zero, $H_c \approx 0.4$T, and an estimate of the ratio (H_{DM}/H_E) using $\tan(2\xi)=(H_{DM}/H_E)$,[17] where $\xi=11^\circ$ is the canting angle, we obtain a value for the in-plane anisotropy field in Sr_2IrO_4, $H_A=1/\sqrt{2}(H_{DM}/H_E)H_c \approx 0.1$T. This estimate compares well with the coercive field ∼0.15T needed to induce an abrupt "spin-flip" transition between AF and WFM phases for H‖b-axis =[010] (see Fig. 4(c)). Additionally, the minimum value for the spin-wave energy at H=0.4 T (see Fig. 4(a)), Δ∼8 cm^{-1} (1 meV), offers a good estimate of the spin-gap energy in Sr_2IrO_4 without the effects of interlayer coupling.

V. SUMMARY

In the field- and temperature-dependent Raman scattering studies of the angle-dependence of spin excitations of Sr_2IrO_4 presented here, we show clear evidence for a magnetic field scale H∼1.5 T above which the in-plane spin dynamics behave in accordance with the predictions of an isotropic, two-dimensional effective S=1/2 Hamiltonian. The field-dependence of spin-wave excitations in this "high field" regime are isotropic, two-dimensional, and solely governed by the interplay between the applied field and the FM component of the spins associated with the DM interaction. However, dramatic deviations from this isotropic and two-dimensional behavior are clearly observed at lower fields, H<1.5 T, manifested, for example, in a highly anisotropic field-dependence of the spin dynamics and interlayer-exchange-split spin-wave modes. Particularly noteworthy is the observation of field-induced magnon soft mode behavior near H_c for a field applied transverse to the FM spin components, $H \perp m_{FM}$, which reveals a continuous spin rearrangement transition at the antiferromagnetic-to-weakly ferromagnetic transition at H_c in Sr_2IrO_4. Our results also show that when the in-plane field is aligned perpendicular to the easy-axis direction of the FM moment, the field dependence of the $\mathbf{q}=0$ spin-wave energy evolves according to $\omega \sim H^{1/2}$ above H_c, i.e., in a manner consistent with a 2D canted antiferromagnet with no spin gap. These studies highlight the importance of considering in-plane anisotropy and interlayer coupling effects on the low energy spin dynamics when interpreting and calculating the low-field magnetic and dynamical properties of Sr_2IrO_4.

Acknowledgments−Research was supported by the National Science Foundation under Grant NSF DMR 14-64090. Work at the University of Kentucky was supported by the National Science Foundation via Grant Nos. DMR-1265162. Work at Argonne National Laboratory (crystal growth and magnetic characterization) was supported by the U.S. Department of Energy Office of Science, Basic Energy Sciences, Materials Science and Engineering Division. We thank Sam Gleason and Greg MacDougall for useful discussions.

[1] F. Wang and T. Senthil, Phys. Rev. Lett. **106**, 136402 (2011).
[2] Y.-Z. You, I. Kimchi, and A. Vishwanath, Phys. Rev. B **86**, 085145 (2012).
[3] Y. Okamoto, M. Nohara, H. Aruga-Katori, and H. Takagi, Phys. Rev. Lett. **99**, 137207 (2007).
[4] B. J. Kim, H. Jin, S. J. Moon, J.-Y. Kim, B.-G. Park, C. S. Leem, J. Yu, T. W. Noh, C. Kim, S.-J. Oh, J.-H. Park, V. Durairaj, G. Cao, and E. Rotenberg, Phys. Rev. Lett. **101**, 076402 (2008).
[5] B. J. Kim, H. Ohsumi, T. Komesu, S. Sakai, T. Morita, H. Takagi, and T. Arima, Science **323**, 1329 (2009), http://www.sciencemag.org/content/323/5919/1329.full.pdf.
[6] D. Pesin and L. Balents, Nat. Phys. **6**, 376 (2010).
[7] A. Shitade, H. Katsura, J. Kuneš, X.-L. Qi, S.-C. Zhang, and N. Nagaosa, Phys. Rev. Lett. **102**, 256403 (2009).
[8] C. H. Kim, H. S. Kim, H. Jeong, H. Jin, and J. Yu, Phys. Rev. Lett. **108**, 106401 (2012).

[9] S. Chikara, O. Korneta, W. P. Crummett, L. E. DeLong, P. Schlottmann, and G. Cao, Phys. Rev. B **80**, 140407 (2009).

[10] G. Cao, J. Bolivar, S. McCall, J. E. Crow, and R. P. Guertin, Phys. Rev. B **57**, R11039 (1998).

[11] M. Ge, T. F. Qi, O. B. Korneta, D. E. De Long, P. Schlottmann, W. P. Crummett, and G. Cao, Phys. Rev. B **84**, 100402 (2011).

[12] F. Ye, S. Chi, B. C. Chakoumakos, J. A. Fernandez-Baca, T. Qi, and G. Cao, Phys. Rev. B **87**, 140406 (2013).

[13] S. J. Moon, M. W. Kim, K. W. Kim, Y. S. Lee, J.-Y. Kim, J.-H. Park, B. J. Kim, S.-J. Oh, S. Nakatsuji, Y. Maeno, I. Nagai, S. I. Ikeda, G. Cao, and T. W. Noh, Phys. Rev. B **74**, 113104 (2006).

[14] J. Kim, D. Casa, M. H. Upton, T. Gog, Y.-J. Kim, J. F. Mitchell, M. van Veenendaal, M. Daghofer, J. van den Brink, G. Khaliullin, and B. J. Kim, Phys. Rev. Lett. **108**, 177003 (2012).

[15] M. K. Crawford, M. A. Subramanian, R. L. Harlow, J. A. Fernandez-Baca, Z. R. Wang, and D. C. Johnston, Phys. Rev. B **49**, 9198 (1994).

[16] S. Fujiyama, H. Ohsumi, T. Komesu, J. Matsuno, B. J. Kim, M. Takata, T. Arima, and H. Takagi, Phys. Rev. Lett. **108**, 247212 (2012).

[17] S. Bahr, A. Alfonsov, G. Jackeli, G. Khaliullin, A. Matsumoto, T. Takayama, H. Takagi, B. Büchner, and V. Kataev, Phys. Rev. B **89**, 180401 (2014).

[18] J.-I. Igarashi and T. Nagao, Phys. Rev. B **88**, 104406 (2013).

[19] J.-I. Igarashi and T. Nagao, Phys. Rev. B **89**, 064410 (2014).

[20] K. Ishii, I. Jarrige, M. Yoshida, K. Ikeuchi, J. Mizuki, K. Ohashi, T. Takayama, J. Matsuno, and H. Takagi, Phys. Rev. B **83**, 115121 (2011).

[21] X. Liu, M. P. M. Dean, J. Liu, S. G. Chiuzbian, N. Jaouen, A. Nicolaou, W. G. Yin, C. R. Serrao, R. Ramesh, H. Ding, and J. P. Hill, Journal of Physics: Condensed Matter **27**, 202202 (2015).

[22] J. Chovan and N. Papanicolaou, The European Physical Journal B - Condensed Matter and Complex Systems **17**, 581 (2000).

[23] A. Gozar, B. S. Dennis, G. Blumberg, S. Komiya, and Y. Ando, Phys. Rev. Lett. **93**, 027001 (2004).

[24] L. Benfatto and M. B. Silva Neto, Phys. Rev. B **74**, 024415 (2006).

[25] L. Benfatto, M. B. Silva Neto, A. Gozar, B. S. Dennis, G. Blumberg, L. L. Miller, S. Komiya, and Y. Ando, Phys. Rev. B **74**, 024416 (2006).

[26] G. M. Sheldrick, Acta Crystallographica Section A **64**, 112 (2008).

[27] STM measurements on the Eu-doped sample (A. Satpathy, private communication) indicate that the Eu concentration is <1% and suggests the possible role of O vacancies at the ∼1% level. Both species in principle are electron donors.

[28] M. F. Cetin, P. Lemmens, V. Gnezdilov, D. Wulferding, D. Menzel, T. Takayama, K. Ohashi, and H. Takagi, Phys. Rev. B **85**, 195148 (2012).

[29] T. Thio, T. R. Thurston, N. W. Preyer, P. J. Picone, M. A. Kastner, H. P. Jenssen, D. R. Gabbe, C. Y. Chen, R. J. Birgeneau, and A. Aharony, Phys. Rev. B **38**, 905 (1988).

[30] R. M. White, R. J. Nemanich, and C. Herring, Phys. Rev. B **25**, 1822 (1982).

[31] M. Cottam and D. Lockwood, *Light scattering in magnetic solids*, Wiley-Interscience publication (Wiley, 1986).

[32] C. Dhital, T. Hogan, Z. Yamani, C. de la Cruz, X. Chen, S. Khadka, Z. Ren, and S. D. Wilson, Phys. Rev. B **87**, 144405 (2013).

[33] T. Thio, C. Y. Chen, B. S. Freer, D. R. Gabbe, H. P. Jenssen, M. A. Kastner, P. J. Picone, N. W. Preyer, and R. J. Birgeneau, Phys. Rev. B **41**, 231 (1990).

[34] G. Jackeli and G. Khaliullin, Phys. Rev. Lett. **102**, 017205 (2009).

[35] H. Horner and C. M. Varma, Phys. Rev. Lett. **20**, 845 (1968).

[36] P. Pincus, Phys. Rev. Lett. **5**, 13 (1960).

[37] S. M. Shapiro, J. D. Axe, and J. P. Remeika, Phys. Rev. B **10**, 2014 (1974).

[38] A. Fainstein, A. Butera, R. D. Zysler, M. Tovar, C. Rettori, D. Rao, S. B. Oseroff, Z. Fisk, S.-W. Cheong, D. C. Vier, and S. Schultz, Phys. Rev. B **48**, 16775 (1993).

[39] C. Wang, H. Seinige, G. Cao, J.-S. Zhou, J. B. Goodenough, and M. Tsoi, Phys. Rev. X **4**, 041034 (2014).

[40] L. M. Levinson, M. Luban, and S. Shtrikman, Phys. Rev. **187**, 715 (1969).

[41] N. Koshizuka and K. Hayashi, Journal of the Physical Society of Japan **57**, 4418 (1988), http://dx.doi.org/10.1143/JPSJ.57.4418.

[42] G. Gorodetsky and B. Lüthi, Phys. Rev. B **2**, 3688 (1970).